Available online at www.sciencedirect.com
SCIENCE DIRECT
Polymer 46 (2005) 7352–7369
polymer
www.elsevier.com/locate/polymer

Toughness of syndiotactic polystyrene/epoxy polymer blends: microstructure and toughening mechanisms

B.B. Johnsen, A.J. Kinloch*, A.C. Taylor

Department of Mechanical Engineering, Imperial College London, South Kensington Campus, London SW7 2AZ, UK

Received 18 April 2005; received in revised form 17 May 2005; accepted 25 May 2005
Available online 5 July 2005

Abstract

Thermoplastic/epoxy blends were formed using an amine-cured epoxy polymer and a semi-crystalline thermoplastic: syndiotactic polystyrene (sPS). Complete phase-separation of the initially soluble sPS from the epoxy occurred via 'reaction-induced phase-separation' (RIPS) or via 'crystallisation-induced phase-separation' (CIPS), depending upon the thermal processing history employed. Dynamic mechanical thermal analysis showed that no sPS was retained dissolved in the epoxy polymer. For RIPS, at concentrations of sPS of up to 8 wt%, the sPS is present solely as spherical particles. However, macro phase-separation, giving a co-continuous microstructure, accompanied by local phase-inversion, dominates the RIPS blends containing more than 8 wt% sPS. In the CIPS blends, the sPS is present as spherulitic particles, and this microstructure does not change over the range of sPS concentrations employed, i.e. from 1 to 12 wt% sPS. The pure epoxy polymer was very brittle with a value of fracture energy, G_{Ic}, of about 175 J/m^2. However, the addition of the sPS significantly increases the value of G_{Ic}, though the toughness of the RIPS and CIPS blends differs markedly. For the RIPS blends, there is a steady increase in the toughness with increasing content of sPS and an apparent maximum value of G_{Ic} of about 810 J/m^2 is obtained for 8–10 wt% sPS. On the other hand, the measured toughness of the CIPS blends increases relatively slowly with the concentration of sPS, and a maximum plateau value of only about 350 J/m^2 was measured in the range of 8–12 wt% sPS. The relationships between the microstructure of the RIPS and CIPS sPS/epoxy blends and the measured fracture energies are discussed. Further, from scanning electron microscopy studies of the fracture surfaces and optical microscopy of the damage zone around the crack tip, the nature of the micromechanisms responsible for the increases in toughness of the blends are identified. For the RIPS blends, (i) debonding of the sPS particles, followed by (ii) plastic void growth of the epoxy matrix are the major toughening micromechanisms. The increase in toughness due to such micromechanisms is successfully predicted theoretically using an analytical model. In the case of the CIPS blends, the increase in the value of G_{Ic} results from (i) crack deflection and (ii) microcracking and crack bifurcation.

Keywords: Polymer blends; Microstructure; Toughening mechanisms

1. Introduction

Thermosetting epoxy polymers are widely used as engineering adhesives and matrices for fibre-composite materials. When cured, epoxy polymers typically possess a high crosslink density. This property leads to good thermal stability and creep resistance, relatively high modulus, and excellent adhesion properties. Unfortunately, the high crosslink density also leads to low ductility and poor fracture toughness, which limits their application as engineering materials.

A very successful route to improve the toughness of thermosetting polymers is to form a blend with a low molecular-weight rubber, where the rubber undergoes phase-separation upon curing the blend [1–4]. The rubber-toughened epoxy often possesses outstanding fracture properties. However, the presence of the rubbery phase may decrease the modulus and the thermal stability of the material, and increase the tendency for water absorption with an accompanying loss of properties at elevated temperatures. Whilst for adhesive applications such decreases in modulus and temperature resistance are usually

* Corresponding author. Tel.: +44 20 7594 7082; fax: +44 20 7594 7017.
E-mail addresses: b.johnsen@imperial.ac.uk (B.B. Johnsen), a.kinloch@imperial.ac.uk (A.J. Kinloch), a.c.taylor@imperial.ac.uk (A.C. Taylor).

0032-3861/$ - see front matter © 2005 Elsevier Ltd. All rights reserved.
doi:10.1016/j.polymer.2005.05.151

of no significance, in matrices for fibre-composites such effects can lead to unacceptable decreases in the properties of the fibre-composite.

An alternative approach to toughening epoxies for use with fibre-composites is based upon blending with a thermoplastic polymer that phase-separates upon curing of the resin [5–11]. The thermoplastic phase has a relatively good thermal stability and low water uptake compared to the rubbers described above. Useful reviews of thermoplastic toughening have been prepared by Pascault and Williams [5], plus Hedrick et al. [12], Hodgkin et al. [13] and Pearson [14]. The thermoplastics employed have typically been functionalized poly(ether sulfone) [6,9–11], poly(ether imide) [7,15–16], polyimide [17], polysulfone [18–19] and polyester [11], which are all amorphous polymers. Semi-crystalline thermoplastics have been used previously, but as preformed particles; and all processing was conducted below the melting point of the thermoplastic [20–22].

The present study employs a thermoplastic/epoxy blend but the toughening agent is a semi-crystalline thermoplastic, namely syndiotactic polystyrene (sPS); as opposed to an amorphous thermoplastic which has been typically employed in previous studies, as noted above. sPS is a relatively new polymer, being synthesized first in 1985 by Ishihara et al. [23], whose semi-crystalline nature results in some excellent properties compared with its atactic, and hence amorphous, counterparts. These properties include a relatively high Young's modulus, very low water uptake, high heat resistance, and good solvent and chemical resistance [24]. One disadvantage is that sPS has to be processed at high temperatures due to its high melting point, T_m, of 270 °C, which is close to the degradation temperature of the polymer [25]. However, the processing of sPS can be facilitated by lowering its melting temperature and viscosity using a curable epoxy/amine system as a reactive solvent [26].

Phase-separation of dissolved sPS from the epoxy occurs via two different routes in sPS/epoxy blends [27], depending upon the thermal processing history that is chosen. First, 'reaction-induced phase-separation' (RIPS) may occur. Here, the reaction of the resin and the curing agent results in the formation of a three-dimensional epoxy network, forcing the sPS out of solution. Secondly, 'crystallisation-induced phase-separation' (CIPS) may be induced. Here, the sPS crystallises before the epoxy network has developed sufficiently to force the sPS out of solution. The thermal processing history of the blend controls the phase-separation process: essentially keeping the temperature of the blend above the crystallisation temperature, T_c, of the sPS before curing will result in RIPS, whilst cooling of the blend to a temperature below T_c before curing will result in CIPS.

The present work describes how varying the thermal history has allowed the effects of RIPS and CIPS on the measured toughness to be quantified. As was observed earlier [28], a significant increase in toughness may be obtained from using relatively small concentrations of sPS thermoplastic in the epoxy polymer. This initial observation is discussed in detail in the present paper. The relationships between the toughness of the RIPS and CIPS blends and their microstructure are explored, and it is clearly demonstrated that the different microstructures may lead to significantly different values of fracture toughness. The toughening micromechanisms responsible for the marked increases in toughness arising from the presence of the sPS phase are then identified, and an analytical model is employed to quantitatively assess the increase in toughness that is observed.

2. Experimental

2.1. Materials

Syndiotactic polystyrene (sPS), 'Dow Questra QA 101', was supplied by Buna Sow Leuna Olefinverbund GmbH, Schkopau, Germany, in the form of coarse granules. The number-average molecular weight, M_n, was 94,100 g/mol, and the weight-average molecular weight, M_w, was 192,000 g/mol [25]. The glass transition temperature, T_g, of the sPS was 97.5–100 °C, and the crystalline melting temperature, T_m, was 270.3 °C, as measured using differential scanning calorimetry [27]. The supplied sPS granules were cryomilled to a fine powder before use in order to accelerate the melting of the sPS in the epoxy resin.

The epoxy resin was a diglycidylether of Bisphenol A (DGEBA), 'DER 330', supplied by Dow Chemicals, Texas, USA, with an epoxy equivalent weight of 191.6 g/mol ($n=0.15$) [25]. The curing agent used was the aromatic diamine 4,4-methylene-bis-(3-chloro-2,6-diethylaniline) (MCDEA). The 'Lonzacure M-CDEA' was supplied by Lonza AG, Basel, Switzerland, and was chosen because of its low reactivity in order to facilitate the high temperature processing of the sPS.

2.2. Polymer blend preparation

Cast sheets of polymer, 6 mm thick, with two different thermal processing histories, were prepared for mechanical testing. In both cases, the epoxy resin and the necessary amount of sPS were first mixed together in a beaker and placed in an oven preheated to 290 °C. The amount of sPS used was varied from 1 to 12 wt%. The sPS/epoxy blend was stirred in the oven using a mechanical stirrer until the sPS melted and dissolved in the epoxy. This typically took 30–45 min depending on the amount of sPS: the higher the concentration of sPS, the longer the time it took to melt and dissolve the sPS into the resin. The blend temperature had at this point normally risen to about 270 °C. Thus, melting of sPS took place below the melting point of the pure sPS since its melting point is significantly depressed in blends with epoxy resin [25]. After mixing, the next steps in the preparation procedures were different for the two thermal

processing histories that were to be followed, depending upon whether RIPS or CIPS blends were being prepared:

(1) RIPS samples were prepared by first lowering the oven temperature to 220 °C after the sPS was dissolved. Approximately 15 min later, the sPS/epoxy blend was mixed with the molten MCDEA curing agent held at a temperature of 220 °C. The ratio between epoxy and MCDEA was 2:1 by weight. The mixing resulted in a liquid sPS/epoxy/MCDEA blend with a temperature of about 240 °C.
(2) CIPS samples were prepared by cooling the sPS/epoxy blend to induce pre-crystallisation of sPS prior to mixing in the MCDEA curing agent. Pre-crystallisation occurred at a blend temperature of 195–185 °C, which is close to the expected crystallisation temperature of sPS. The blend, which was initially transparent, turned milky-white and became more viscous at this point. A few minutes later, the blend was mixed with the molten MCDEA, which had been held at a temperature of 220 °C.

After either of these steps, the sPS/epoxy/MCDEA blends were stirred for two minutes before they were poured into a preheated mould and cured for 1 h. The RIPS blends were then cured at 230 °C, whilst the CIPS blends were cured at 220 °C. The oven was then switched off and the mould was left in the oven to cool slowly overnight, after which time the sheet of polymer was removed from the mould. Sheets of pure epoxy were prepared according to the procedure for both the RIPS and the CIPS sheets, but with the omission, of course, of the sPS. (It should be noted that in the previous work [28] all samples had been cured at 220 °C. However, it was found that, in some cases, this led to a mixed RIPS plus CIPS microstructure, rather than a pure RIPS material. Hence, in the present studies, the curing temperature was increased to 230 °C for all the RIPS samples.)

2.3. Fracture testing

The compact tension test was used to determine the fracture toughness, K_{Ic}, of the polymers. Specimens were machined from the sheets, and the fracture toughness was determined according to the relevant standard [29], using a displacement rate of 1 mm/min and a test temperature of 21 °C. Four replicate specimens were tested for each blend composition. The machined notch was sharpened by drawing a razor blade across the notch tip before testing. All the specimens failed by unstable crack growth, and hence only a single, initiation, value of the fracture toughness was obtained from each specimen. The fracture energy, G_{Ic}, was calculated from the fracture toughness using:

$$G_{Ic} = \frac{K_{Ic}^2}{E}(1-\nu^2) \quad (1)$$

where E is the modulus of elasticity obtained from the dynamic mechanical thermal analysis studies, and ν is the Poisson's ratio of the polymer, taken to be 0.35 [30].

2.4. Material characterisation

The fracture surfaces of the specimens were investigated using scanning electron microscopy (SEM). A JEOL 'JSM-5300' scanning microscope was used, and all specimens were coated with a thin layer of sputtered gold before analysis. Surface roughness measurements of the fracture surfaces were performed using a Form Talysurf series 2 from Taylor Hobson. A sharp stylus with a tip radius of 2.5 μm, attached to a cantilever, was drawn across the surface at a constant speed for a set distance. Five measurements with a traverse length of 4 mm were performed perpendicular to the direction of the crack growth. The average roughness, R_a, of the line profiles was calculated.

Thin sections, approximately 60–80 nm thick, of the blends were cryo-microtomed for subsequent examination using transmission electron microscopy (TEM). The TEM was performed using a JEOL 'JEM-2000FX II' electron microscope at an acceleration voltage of 200 kV.

The blends were also investigated using reflection optical microscopy (ROM) and transmission optical microscopy (TOM). Before optical microscopy, the specimens were polished using standard petrographic methods as described by Holik et al. [31]. This process involves cutting a piece of the specimen and embedding it in a low viscosity epoxy. The specimen is then polished using aluminium oxide paper, whilst cooling the specimen with water. Different polishing cloths and diamond pastes of increasing fineness are employed until the required surface finish for ROM is obtained. For analysis using TOM, the polished piece is mounted onto a glass slide, with the polished side face-downwards, and then polished again until the required thickness, of approximately 40 μm, and surface finish are obtained.

Dynamic mechanical thermal analysis (DMTA) was performed by testing bars 48 mm × 3 mm × 2 mm in size in the three-point-bending mode at 1 Hz using a 'Tritec 2000 DMTA' from Triton Technology. The storage modulus, loss modulus and loss factor, tan δ, were calculated as a function of temperature. The glass transition temperature, T_g, was taken to be the temperature at which the peak value of tan δ occurred. Note that DMTA gave somewhat higher T_g values than those obtained using differential scanning calorimetry, e.g. in Ref. [27].

2.5. Double-notch four-point-bend testing

To investigate the toughening micromechanisms of the polymer blends a double-notch four-point-bend (DN-4PB) technique was employed [32–36]. When the specimen is loaded in four-point bending, two almost identical

pre-cracks experience nearly identical levels of stress. One of the cracks will propagate unstably, thus resulting in fracture, while the other crack will not propagate. After fracture, the 'nearly-critical' damage zone that has developed at the tip of the crack which did not propagate, can be investigated using microscopic techniques such as TEM and TOM. This damage zone can give information about the deformation micromechanisms taking place in the polymer blend, such as deformation, elongation or cavitation of second-phase particles, or plastic deformation of the polymer matrix.

The DN-4PB technique was performed by broadly following the procedure of Sue [32,33]. Rectangular specimens of size 62 mm × 8.5 mm × 4.2 mm were cut from the sheet materials, and two notches were machined. Two nearly identical pre-cracks were made by gently tapping a razor blade into each of the two notches. The ratio between the final crack length, a, and the specimen width, w, was held in the range 0.3–0.7. The distance between the two cracks was 5.6 mm. The specimens were loaded in four-point bending, using a rate of displacement of 1 mm/min, and a test temperature of 21 °C.

2.6. Plastic zone size

Microscopy of the sub-critical crack in the DN-4PB specimens allows the size of the plastic zone at the crack tip to be measured experimentally. This value can be compared to the theoretical size of the plastic zone ahead of the crack tip, calculated assuming linear-elastic fracture-mechanics (LEFM) behaviour. Under plane-strain conditions and assuming that the zone is circular [37] as proposed by Irwin, the radius of the plastic zone, r_y, can be calculated using the relationship:

$$r_y = \frac{1}{6\pi}\left(\frac{K_{Ic}}{\sigma_y}\right)^2 \quad (2)$$

where K_{Ic} is the fracture toughness and σ_y is the tensile yield stress of the polymer.

However, in many polymers the plastic zone ahead of the crack tip is not circular, and is better modelled as a line-zone using the Dugdale analysis [37]. The length of the plastic zone, R, ahead of the crack tip can be estimated using the relationship:

$$R = \frac{\pi}{8}\left(\frac{K_{Ic}}{\sigma_y}\right)^2 \quad (3)$$

Under plane-strain conditions, the crack-opening displacement at the crack tip is given by [37]:

$$\delta_t = \frac{K_{Ic}^2}{E\sigma_y}(1-\nu^2) \quad (4)$$

In the present work, the compressive yield stress, σ_{yc}, of the unmodified epoxy polymer, cured at 220 °C, is 97.8 MPa [38], and the tensile yield stress, σ_y, can be calculated from the compressive yield stress [39]; giving a value of σ_y = 77.3 MPa.

3. Fracture properties

The dependence of the fracture toughness, K_{Ic}, at the onset of crack growth as a function of the concentration of the thermoplastic sPS is shown in Fig. 1, for the RIPS and the CIPS blends. These data are also summarised in Table 1.

The pure epoxy polymer is very brittle with K_{Ic} values of 0.55 and 0.73 $MNm^{-3/2}$, after curing at 220 and 230 °C, respectively, which is typical of a brittle thermosetting polymer [10,30]; with only a small difference being seen due to the slightly different cure temperatures. The addition of only 1 wt% sPS gives an immediate increase in toughness. A value of about 0.8 $MNm^{-3/2}$ is recorded for both the RIPS and for the CIPS blends.

However, above 3 wt% sPS the measured fracture toughness for the RIPS and CIPS blends differs markedly. For the RIPS blends there is a steady increase in toughness with increasing content of sPS. A maximum value of K_{Ic} = 1.42 $MNm^{-3/2}$ is obtained at 8 wt% sPS, see Fig. 1; with the initial relationship between K_{Ic} and wt% sPS being linear. Above 8 wt% of sPS, the toughness starts to decrease somewhat. The measured toughness of the CIPS blends increases only slightly for concentrations of sPS above 1 wt% sPS. Hence, the toughness of the CIPS blends does not reach a maximum value in the same way as for the RIPS blends, but is approximately constant, within experimental error, over the range from 1 to 12 wt% of sPS used in the present work. For example, a value of K_{Ic} = 0.83 $MNm^{-3/2}$ was measured for the CIPS blend containing 1 wt% of sPS, and a K_{Ic} of 0.93 $MNm^{-3/2}$ was measured for the CIPS blend containing 8 wt% sPS. In addition, the measured toughness values are much lower than those for the RIPS blends. This is clearly shown by comparing the K_{Ic} values at 8 wt% sPS. At this concentration, the value of K_{Ic} for the RIPS blend is more than 50% higher than that for the CIPS blend.

There are several noteworthy points from the above

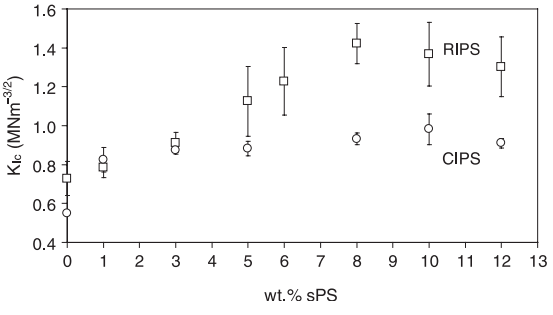

Fig. 1. Fracture toughness, K_{Ic}, of the sPS/epoxy blends. ('□' represents the pure epoxy and RIPS blends cured at 230 °C, while '○' represents the pure epoxy and CIPS blends cured at 220 °C. Error bars are ±1 standard deviation).

Table 1
Mechanical properties and glass transition temperatures of the sPS/epoxy blends

Sample type	Content of sPS (wt%)	Fracture toughness, K_{Ic} ($MNm^{-3/2}$)	Modulus, E (GPa)	Glass transition temperature, T_g (°C)	
				Epoxy-phase	sPS-phase
Epoxy (230 °C)[a]	n/a[b]	0.73	2.07	181[c]	n/a
RIPS	1	0.79	2.16	183	99
	3	0.91	2.15	182	101
	5	1.13	2.23	184	101
	6	1.23	2.13	183	101
	8	1.42	2.22	183	102
	10	1.37	2.00	184	101 + 114[d]
	12	1.30	2.03	183	101 + 117[d]
Epoxy (220 °C)[e]	n/a	0.55	2.16	179	n/a
CIPS	1	0.83	2.20	179	–
	3	0.87	2.23	176	~140[f]
	5	0.88	2.17	179	~140[f]
	8	0.93	2.19	178	~140[f]
	10	0.98	2.19	178	~140[f]
	12	0.91	2.19	180	~140[f]
sPS	100	n/d[g]	2.59	n/a	114

[a] The pure epoxy and the RIPS blends were cured at 230 °C.
[b] Not applicable.
[c] The typical reproducibility of the T_g values was ±1 °C.
[d] Is present as a shoulder on the main peak at 115 ± 1 °C.
[e] The pure epoxy and the CIPS blends were cured at 220 °C.
[f] No separate peak was detected for the sPS phase, but there was a shoulder on the tan δ peak of the epoxy phase, typically starting at a temperature of about 105 °C.
[g] Not determined. ($K_{Ic} = 0.34\ MNm^{-3/2}$ is quoted in Ref. [28].)

results. First, the significant increase in the fracture toughness upon the addition of only very small amounts of sPS. Secondly, there is a significant difference between the fracture performance of the RIPS and the CIPS blends. Thirdly, previous thermoplastic/epoxy blends have employed amorphous, rather than semi-crystalline, thermoplastics to improve the fracture performance of polymer blends. However, large increases in the value of K_{Ic} are generally only measured when a co-continuous or phase-inverted microstructure is formed, and 20–30 wt% of amorphous thermoplastic is typically required to achieve the optimum mechanical properties [11,13,15,16].

4. Microstructure of the sPS/epoxy blends

4.1. Introduction

The cured sPS/epoxy blends were investigated using reflection optical microscopy (ROM) and transmission electron microscopy (TEM) of the blends, and scanning electron microscopy (SEM) of the fracture surfaces to determine the microstructure. The blends prepared by the 'reaction-induced phase-separation' (RIPS) mechanism gave a very different microstructure than the blends prepared by the 'crystallisation-induced phase-separation' (CIPS) mechanism. Thus, the thermal history of the blends has a significant effect on the microstructure.

Microscopy of the unmodified epoxy showed that a homogeneous thermoset is formed. The fracture surface of the pure epoxy polymer is virtually flat and featureless, which is typical of a brittle thermosetting polymer [22], and shows that little plastic deformation has occurred during fracture.

4.2. The RIPS blends (containing 1–8 wt% sPS)

Optical microscopy of the RIPS blends showed that the thermoplastic sPS phase is present as particles that are homogeneously distributed through the epoxy matrix, as shown in Fig. 2. These particles are a few micrometres in diameter, with a relatively narrow size distribution. A transmission electron micrograph of a microtomed section of the RIPS blend containing 6 wt% sPS is shown in Fig. 3. The second-phase sPS particles are formed as the result of the gelation of the epoxy polymer during the curing reaction, leading to the RIPS of the sPS; with the phase-separation occurring prior to gelation [27]. At relatively low concentrations of sPS, the particles are typically 1–3 μm in diameter, but the number and the size of the particles increases with the concentration of sPS, leading to particles in the range 2–4 μm for the RIPS blend containing 8 wt% sPS, see Fig. 4, where the maximum value of fracture toughness is reached.

The fracture surfaces of the RIPS blends, see Fig. 4, show clearly the spherical sPS particles. There are also many sites in the fracture surfaces where particles are missing; either because they are trapped within a cavity on the opposite

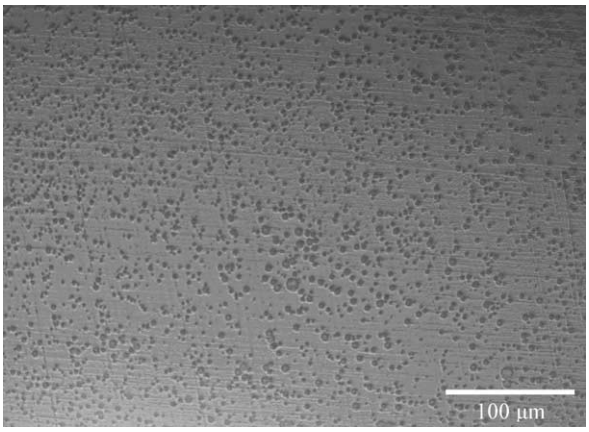

Fig. 2. Reflection optical micrograph of a polished sample of the RIPS blend containing 8 wt% sPS.

fracture surface, or because they have fully debonded from the epoxy matrix and subsequently fallen from the fracture surface. These micrographs also show that the sPS particles appear to be poorly bonded to the epoxy. The surfaces of the particles are clean, with no residual epoxy attached to them. Polystyrene has a relatively low surface free energy compared to the epoxy matrix and will not be readily wetted by, or adhere well to, the epoxy [40]. Poor adhesion is therefore to be expected between the thermoplastic phase and the epoxy matrix, and hence the sPS can easily debond from the epoxy matrix during fracture.

4.3. The RIPS blends (containing above 8 wt% sPS)

In the concentration range above 8 wt% sPS in the RIPS blends, the sPS is mainly present as a co-continuous phase in the epoxy matrix and 'macro phase-separation' occurs; i.e. the sPS phase now has dimensions on the order of millimetres, as shown in Figs. 5 and 6a. The co-continuous

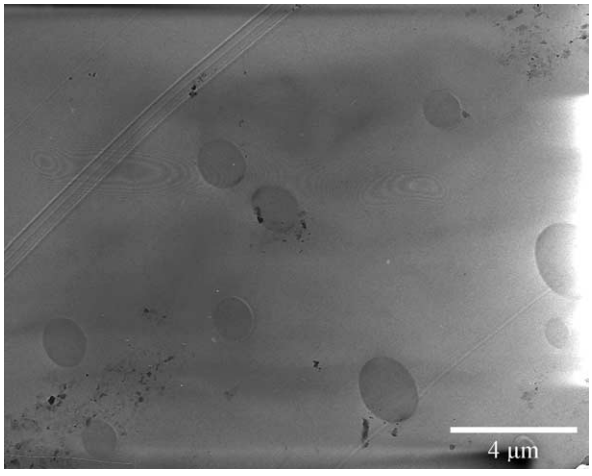

Fig. 3. Transmission electron micrograph of the RIPS blend containing 6 wt% sPS.

macro-phase of sPS has a large number of approximately spherical epoxy particles within it, as shown in Fig. 5. These particles are present throughout the macro phase-separated sPS, indicating that there is a local phase-inversion. SEM shows that these phase-inverted epoxy particles are typically 10–50 μm in diameter, see Fig. 6(b).

In addition to the macro phase-separation, above 8 wt% sPS, the RIPS blends still contain spherical sPS particles in the epoxy matrix, with a diameter of a few micrometres, as was observed for lower concentrations of sPS.

This macro phase-separation of sPS during RIPS has been observed previously [27], and takes places in a critical region between 8–15 wt% sPS. Note that some, but very little, macro phase-separation of sPS was also observed at 8 wt% sPS, using optical microscopy. This suggests that 8 wt% sPS is close to the maximum concentration where only spherical particles of sPS will be formed during the reaction-induced phase-separation of the sPS, under the conditions used in these studies.

4.4. The CIPS blends

The CIPS blends, where the sPS is pre-crystallised before curing the epoxy, have a microstructure that is very different from that of the RIPS blends. Scanning electron microscopy of the fracture surfaces did not show the microstructure of the blends clearly, see Fig. 7, but did reveal that the CIPS blends did not contain any of the spherical particles seen in the RIPS blends. However, the microstructure of the CIPS blends was identified using a combination of optical and transmission electron microscopy.

Fig. 8 shows a reflection optical micrograph of a polished surface of the CIPS blend containing 8 wt% sPS. The darker, particulate, areas in the micrograph are the sPS phase. The sPS domains vary greatly in size, and are much larger than those observed for the RIPS blends. The smallest domains have a diameter around 15 μm, while the largest domains have a diameter of approximately 300 μm.

TEM of the CIPS blend containing 8 wt% sPS, see Fig. 9, shows that the sPS is present as spherulites with a thin fibrillar substructure, the thickness of the fibrils being as low as a few nanometres. Crystallites which have a spherulitic microstructure with an open and pronounced fibrillar substructure have previously been observed in sPS/DGEBA blends [27]. No macro phase-separation of sPS was observed for the CIPS blends at any concentration of sPS.

5. Dynamic mechanical thermal analysis (DMTA) studies

5.1. Introduction

Dynamic mechanical thermal analysis (DMTA) was used to determine the modulus, E, and the glass transition

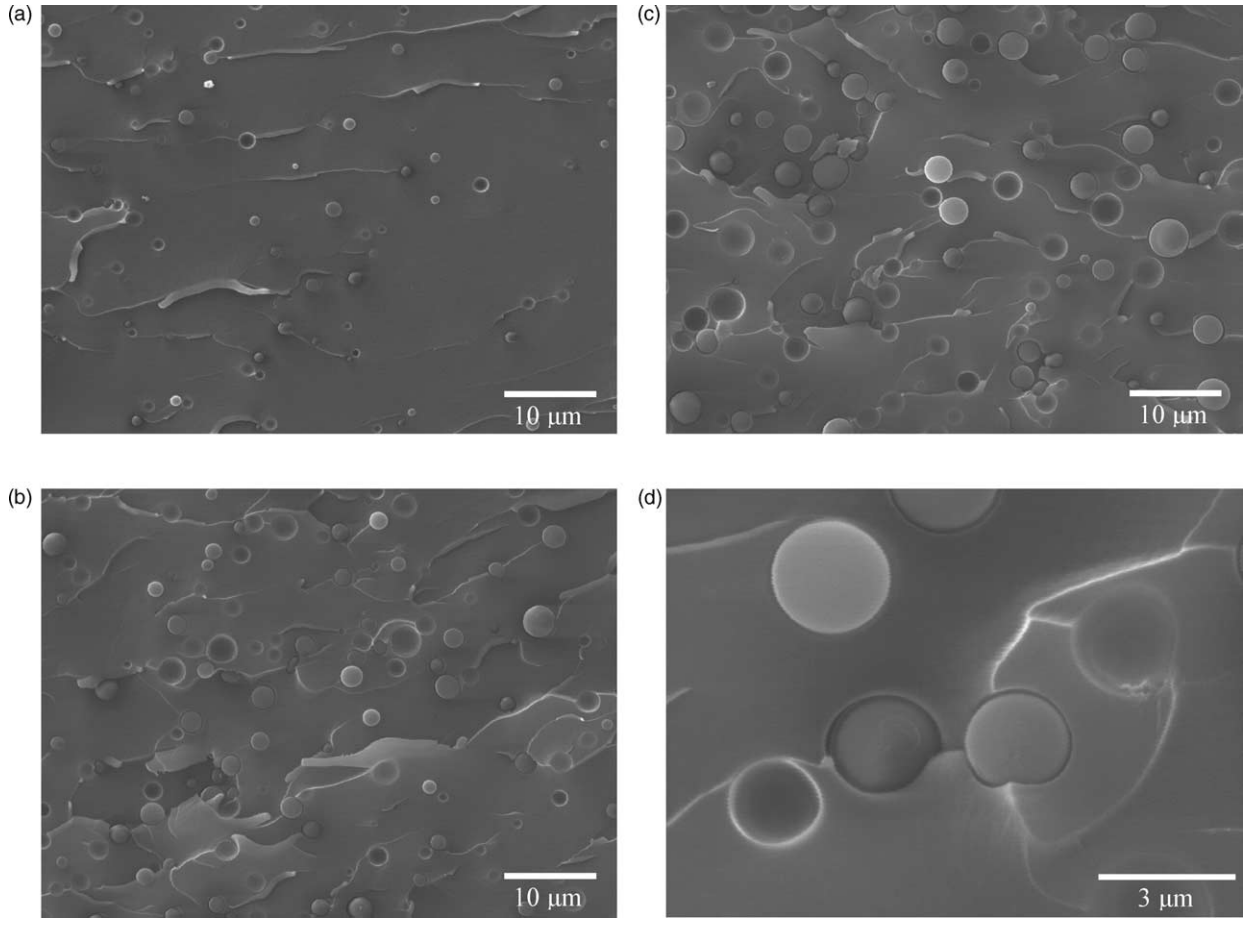

Fig. 4. Scanning electron micrographs of the fracture surfaces of RIPS blends, showing spherical sPS particles in the epoxy matrix for samples containing (a) 1 wt% sPS; (b) 5 wt% sPS; and (c) 8 wt% sPS, and (d) magnified view showing voids around the particles for the sample containing 8 wt% sPS. (The direction of the crack growth is from right to left).

temperature, T_g, of the epoxy and sPS phases present in the sPS/epoxy blends, see Table 1. The variation of modulus and loss factor, tan δ, with temperature for the cured epoxy polymer, pure sPS, and some of the RIPS and CIPS blends are shown in Fig. 10.

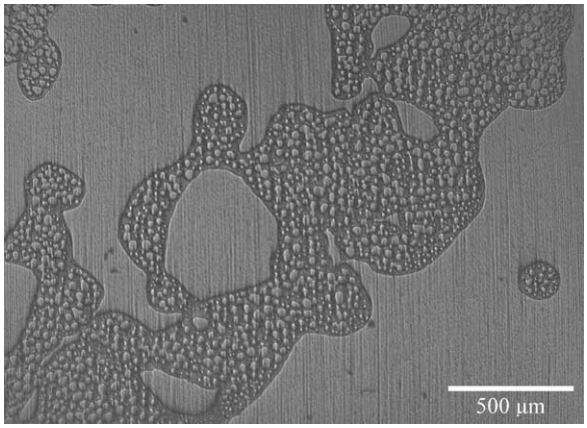

Fig. 5. Reflection optical micrograph of a polished sample of the RIPS blend containing 10 wt% sPS.

5.2. Glass transition temperature

5.2.1. Epoxy T_g

The DMTA results show that the T_gs of the pure epoxy polymer and of the epoxy matrix in the sPS/epoxy blends were in the range 181 ± 3 °C, independent of the concentration of sPS and the thermal processing history; i.e. whether RIPS or CIPS, and hence independent of the blend microstructure. The sPS has totally phase-separated in the cured blends. Thus, no sPS is present in the epoxy matrix; or indeed in the phase-inverted epoxy particles within the macro-phase of sPS for the RIPS blends containing more than 8 wt% sPS.

5.2.2. The RIPS blends (containing 1–8 wt% sPS)

The RIPS blends with a concentration up to 8 wt% sPS, gave a T_g of the sPS phase at 101 ± 1 °C, in addition to the T_g of the epoxy matrix, as shown in Fig. 10 and Table 1. In contrast, the T_g of the pure sPS was 114 ± 1 °C. This discrepancy will be discussed below.

5.2.3. The RIPS blends (containing above 8 wt% sPS)

For the RIPS blends containing 10 and 12 wt% of sPS the

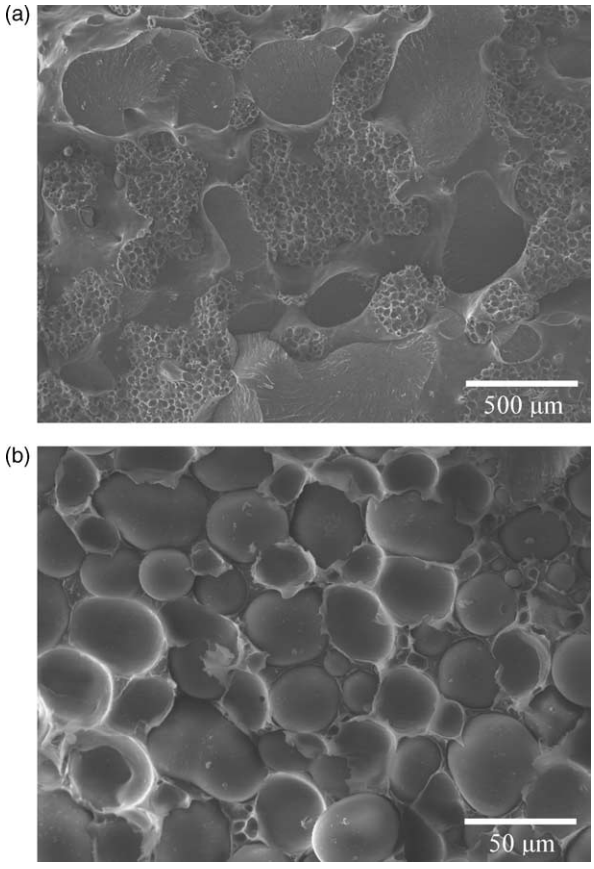

Fig. 6. Scanning electron micrographs of fracture surface of the RIPS blend containing 10 wt% sPS, showing (a) the macro phase-separation of sPS; and (b) local phase-inversion giving epoxy particles in the macro separated sPS phase. (The direction of the crack growth is from right to left).

DMTA results are somewhat more complex. The sPS phase possessed a main tan δ peak, representing the main T_g of this phase, of 115 ± 1 °C, as shown in Table 1. However, a shoulder was observed to be present on this peak at 101 °C, see Fig. 11.

The RIPS blends containing 1–8 wt% of sPS possessed the sPS phase solely in the form of well-dispersed spherical particles. However, for the RIPS blends containing 10–12 wt% of sPS, the sPS phase-separated to give (i) a co-continuous macro-sized phase, with local phase-inversion within the sPS macro-phase, and (ii) a relatively low concentration of spherical particles of phase-separated sPS. Thus, these observations from the various microscopy studies are clearly confirmed by the DMTA results. The weak-intensity shoulder at 101 °C may be assigned to the particulate phase-separated sPS. This assignment is in full agreement with that for the similar particulate morphology of the sPS phase seen in the RIPS blends containing 1–8 wt% sPS. The main broad T_g peak seen at 115 °C in the RIPS blends containing 10 and 12 wt% of sPS may be assigned to the co-continuous, macro-size, phase-separated sPS, which also has within it local phase-inversion giving rise to epoxy particles. Note that the T_g of the sPS in the

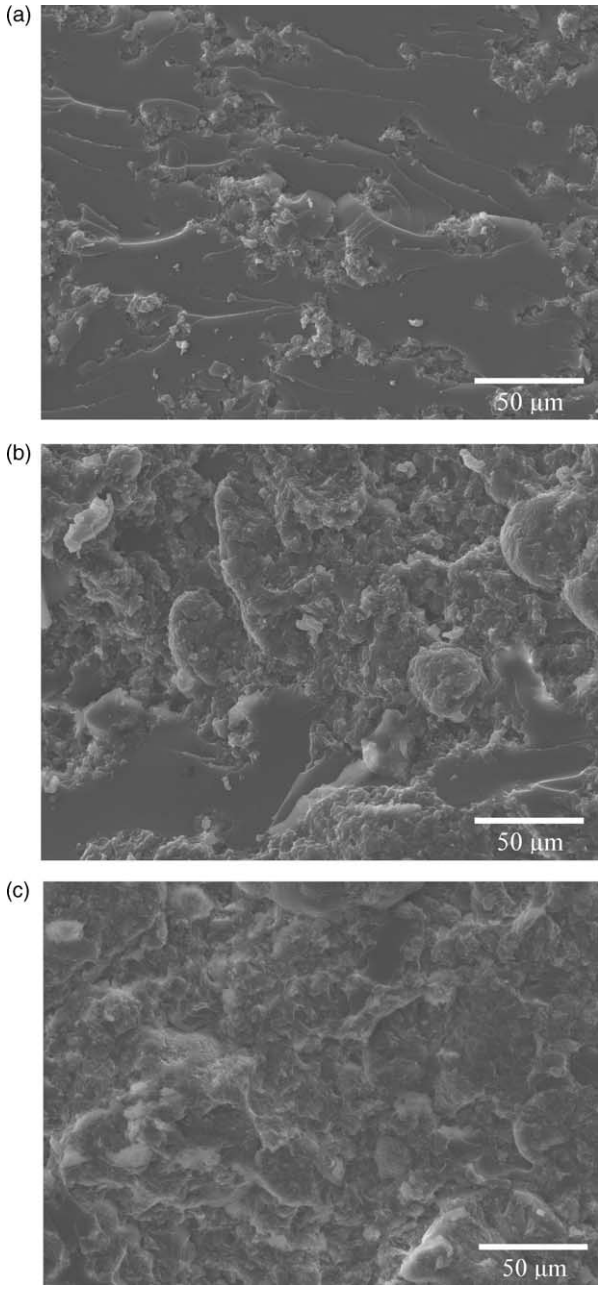

Fig. 7. Scanning electron micrographs of the fracture surfaces of the CIPS blends. Samples contain: (a) 1 wt% sPS; (b) 8 wt% sPS; and (c) 12 wt% sPS. (The direction of the crack growth is from right to left).

macro-phase is not significantly different to that of pure sPS, see Table 1.

5.2.4. The CIPS blends

For the CIPS blends, no clear T_g could be observed for the sPS at around 114 °C. However, a shoulder on the lower-temperature side of the tan δ peak for the epoxy polymer was observed at approximately 105 °C, see Fig. 12. The intensity of this shoulder is dependent on the concentration of sPS, with higher concentrations resulting in a more intense shoulder. Indeed, if the pure epoxy tan δ data are

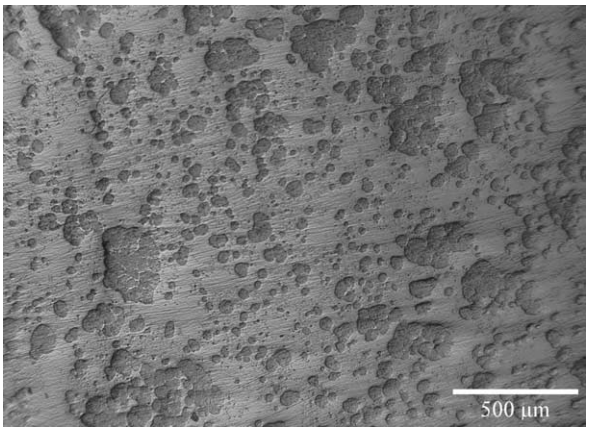

Fig. 8. Reflection optical micrograph of a polished sample of the CIPS blend containing 8 wt% sPS. The darker areas are domains that contain spherulitic sPS, whereas the brighter area is the epoxy matrix.

subtracted from that of the results for the CIPS blends a broad peak emerges around a maximum temperature of about 143 °C for the 5 wt% blend and 135 °C for the 12 wt% blend. Thus, it appears that the T_g of the spherulitic sPS phase in the CIPS blend has a significantly higher T_g than that of the pure sPS of 114 °C.

5.2.5. The T_gs of the sPS phases in the RIPS and CIPS blends

From the above discussion, three noteworthy points emerge:

(1) The RIPS blends, with a concentration up to 8 wt% sPS, give a T_g of the sPS spherical, particulate phase of 101 °C. In contrast, the T_g of the pure sPS was 114 °C.
(2) The main broad T_g peak seen at 115 °C in the RIPS blends containing 10 and 12 wt% of sPS may be assigned to the co-continuous, macro-sized, phase-separated sPS, which also has within it local phase-inversion giving rise to epoxy particles. This value corresponds to that of the T_g of pure sPS.
(3) The T_g of the spherulitic sPS phase in the CIPS blend has a significantly higher T_g of about 140 °C compared to that of the pure sPS of 114 °C.

Fig. 9. Transmission electron micrograph of the CIPS blend containing 8 wt% sPS.

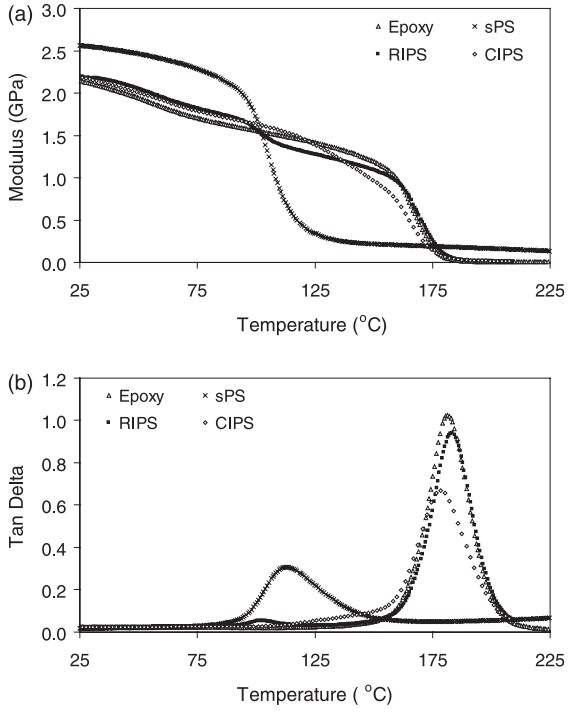

Fig. 10. DMTA scans of the cured epoxy, pure sPS and sPS/epoxy blends showing the values of (a) modulus; and (b) tan δ. (The pure epoxy was cured at 220 °C, as in the preparation of the CIPS sPS/epoxy blends. The RIPS and CIPS blends contain 8 wt% sPS).

These differences in the T_gs of the sPS phase compared to the pure sPS are most likely to arise from the degree of crystallisation of the sPS phase in the blends being different to that of the pure sPS. This raises several interesting points. Firstly, the sPS phases may well exhibit different crystalline melting temperatures, T_m, to that of the pure sPS, and this effect might well lead to different T_g values for the sPS phases in the blends, as compared to the pure sPS polymer [41]. Indeed, it has been reported [42] that the T_g of amorphous sPS was about 10 °C lower than that of the

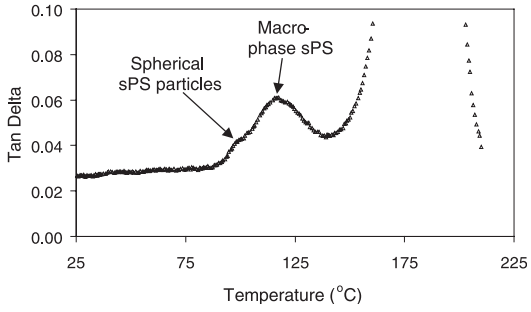

Fig. 11. DMTA scan of tan δ versus temperature of the RIPS blend containing 12 wt% sPS.

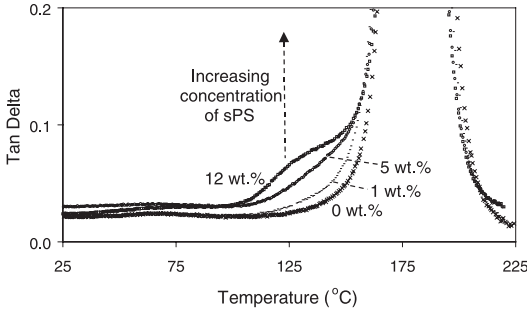

Fig. 12. DMTA scans of tan δ versus temperature of the CIPS blends and the pure epoxy cured at 220 °C. The blends contain from 1 to 12 wt% sPS.

amorphous regions in sPS with a crystallinity of approximately 60%. However, in the present studies, the epoxy matrix starts to degrade at around 275 °C, which masks the melting of the sPS in the blends, at about 270 °C. Secondly, it has been reported that the degree of crystallinity of the pure sPS used in the present studies was about 60% [27], whilst the sPS particles in the RIPS blends are relatively amorphous [43]. This observation is supported by the transmission optical micrographs obtained using polarized light, as shown in Fig. 13(a), which demonstrate that the sPS particles in the RIPS blends have low crystallinity, and

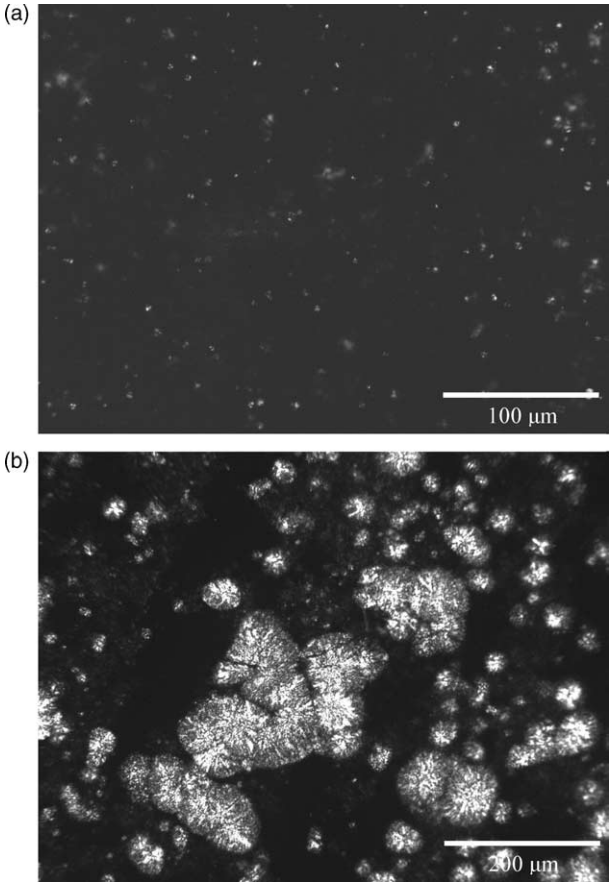

Fig. 13. Transmission optical micrographs obtained using polarized light of the (a) RIPS and (b) CIPS blends containing 8 wt% sPS.

hence, they are difficult to detect. Thirdly, turning to the CIPS blends, the relatively high T_g of the spherulitic sPS phase may also be attributed to the degree of crystallinity in this sPS phase, since the sPS is crystallised before the curing agent is added, and hence before any curing of the epoxy matrix occurs. Thus, the sPS phase in the CIPS blends is able to attain a highly crystalline state, and therefore, a high T_g of the amorphous regions is measured. Indeed, the spherulitic sPS structure in the CIPS blends can clearly be seen in Fig. 13(b), which would indicate a relatively high crystallinity. Further, it has also been reported [27] that the crystallinity of the sPS phase in uncured sPS/DGEBA blends, which also has a spherulitic structure, is increased with decreased content of sPS. This would result in a higher T_g being measured for the sPS phase at lower concentrations of added sPS, which is, indeed, observed for the present CIPS blends, see Section 5.2.4.

Thus, the most likely explanation for the different values of T_g for the sPS phases in the RIPS and CIPS blends is due to the degree of crystallisation of the sPS. The crystallinity increases as the sPS phase changes in nature from particulate (in the RIPS blends at relatively low sPS concentrations) to co-continuous (in the RIPS blends at relatively high sPS concentrations) to spherulitic (in the CIPS blends).

5.3. Modulus data

The moduli of the pure epoxy, and of all of the sPS/epoxy blends, were in the range 2.18 ± 0.05 GPa, see Table 1. The only significant exceptions to this were the macro phase-separated 10 and 12 wt% RIPS blends, which possessed a modulus of around 2.01 GPa. The modulus of the pure sPS was somewhat higher at 2.61 GPa. These data show that the modulus of the epoxy polymer is not normally decreased upon addition of sPS, except in cases where macro phase-separation of the sPS takes place. Indeed, using a rule of mixtures analysis, the modulus of the blends would be expected to increase slightly with increasing concentrations of sPS. However, the predicted increase is small, and would be expected to be within the experimental scatter. It should also be noted that the small reduction in modulus for the macro phase-separated blends is not unexpected, as there is little or no adhesion between the large domains of sPS and the epoxy matrix.

6. Toughening micromechanisms

6.1. Values of the fracture energy

The fracture energy, G_{Ic}, was calculated from the fracture toughness, K_{Ic}. These values are shown as a function of the concentration of sPS in Fig. 14. The pure epoxy polymer has a value of G_{Ic} of 120 ± 5 J/m^2 when cured at 220 °C and a value of about 230 ± 50 J/m^2 when cured at 230 °C. (It will

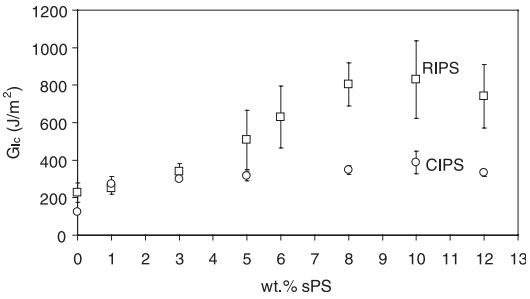

Fig. 14. Fracture energy, G_{Ic}, of the sPS/epoxy blends. ('□' represents the pure epoxy and RIPS blends cured at 230 °C, while '○' represents the pure epoxy and CIPS blends cured at 220 °C. Error bars are ±1 standard deviation).

be recalled that the CIPS blends are cured at 220 °C, but the RIPS blends are cured at 230 °C. Thus, the 'control' pure epoxy polymer appropriate to either of these blends does possess a somewhat different value of G_{Ic}.)

The RIPS blends exhibit far higher fracture energies than the CIPS blends, at thermoplastic contents of 5 wt% or more, see Fig. 14. The RIPS blends give a steady increase in G_{Ic} from the pure epoxy value of 230 J/m^2 to an apparent maximum of about 810 J/m^2 at 8–10 wt% sPS. Upon macro phase-separation of the sPS starting at about 10 wt% of sPS, the fracture energy of the RIPS blends does appear to decrease slightly. For the CIPS blends, the fracture energy of the corresponding pure epoxy polymer is 120 J/m^2 and the fracture energy at 5 wt% of sPS is about 320 J/m^2, with a maximum plateau value of about 350 J/m^2 being measured over the range of 8–12 wt% sPS.

Thus, there are two noteworthy features. First, the strong dependence of the value of G_{Ic} due to (i) the concentration of sPS in the blend and (ii) the microstructure of the sPS/epoxy blend. Secondly, the very marked increase in toughness that arises in the RIPS blends for a relatively low concentration of sPS in the epoxy polymer. For example, the toughness was increased from 230 J/m^2 for the pure epoxy to a value of 800 J/m^2 for the 8 wt% sPS/epoxy blend.

6.2. Toughening micromechanisms

6.2.1. Toughening micromechanisms in the pure epoxy

The pure epoxies cured at 220 and 230 °C have fracture energies of 120 and 230 J/m^2, respectively. These values are typical of brittle thermosetting epoxy polymers [10,30]. Microscopy showed that the fracture surfaces are flat and virtually featureless, which is typical of a brittle thermosetting polymer [22], indicating that little plastic deformation has occurred during fracture.

The double-notch four-point bending (DN-4PB) technique was used to investigate the toughening micromechanisms. Optical microscopy was used to examine the damage zone formed at the sub-critical crack tip of the DN-4PB specimens. The sub-critical pre-crack in the pure epoxy specimen was straight, perpendicular to the direction of the applied tensile stress, and it was not deflected. No evidence of plastic deformation of the epoxy matrix was found at the damaged crack tip. Polarised light TOM showed that the plastic zone was approximately 13 μm long by 3 μm wide. The theoretical size of the plastic zone ahead of the crack tip can be calculated as discussed above. The shape of the plastic zone clearly resembled that proposed by the Dugdale model, and Eq. (3) gives a plastic line-zone length, R, of 20 μm, while Eq. (4) gives a crack-opening displacement of 2 μm. These theoretical values, therefore, agree quite well with the measured size of the plastic zone.

6.2.2. Toughening micromechanisms of the RIPS blends (1–8 wt% sPS)

For the RIPS blends containing 1–8 wt% sPS, the sPS phase is present as spherical particles, see Fig. 4 for example. The number and the size of the particles increase significantly as the concentration of sPS is increased. For example, the diameter of the particles increases from 1 to 3 μm at low concentrations of sPS, up to 2–4 μm at 8 wt% sPS. These increases are accompanied by an increase in the fracture energy, from the pure resin value of 230 J/m^2 to a value of 800 J/m^2 at 8 wt% sPS. This represents an increase in the fracture energy of 350% for the addition of only 8 wt% of the thermoplastic.

Scanning electron microscopy of the fracture surfaces shows that debonding has occurred between the spherical sPS particles and the epoxy matrix. Indeed, cavities are present around the sPS particles, see Fig. 4(d). These cavities might at first be considered to arise from differences in the thermal expansion coefficients, resulting in differential contraction of the thermoplastic and thermoset polymers during cooling of the blend from its curing temperature. However, this consideration is not supported by transmission electron microscopy, see Fig. 3 for example, which shows that no such cavities were present prior to undertaking the fracture tests. These observations are confirmed by reports in the literature, where no cavities were observed in other thermoplastic/epoxy blends prior to fracture [10]. Indeed, the literature reveals that the epoxy tends to shrink onto the particles during curing, rather than away from them, and hence there are no cavities formed prior to fracture testing. Thus, the cavities clearly arise from debonding of the particles during fracture of the specimens, which is then followed by plastic void growth of the epoxy matrix. These events are all encouraged by the presence of the triaxial stresses at the crack tip under the plane-strain constraint conditions [22]. Considering the debonding mechanism, then the adhesion between the polystyrene and the epoxy would be expected to be relatively poor since polystyrene has a low surface free energy compared to the epoxy resin, which leads to very poor wetting of the polystyrene particles by the epoxy and only weak adhesion forces acting across the interface [30]. Thus, the sPS particles can easily debond from the epoxy matrix during fracture, as shown by the lack of residual epoxy on the

surfaces of the sPS particles, see Fig. 4 for example. The debonding of the particles then enables plastic void growth of the epoxy polymer to occur. Hence, it appears that the increase in toughness in the sPS/epoxy blends prepared via the RIPS procedure arises from the energy dissipated by debonding of the spherical sPS particles and, more importantly, the energy associated with plastic void growth in the epoxy polymer.

Transmission electron microscopy of the sub-critical crack in the DN-4PB specimens was used to further confirm that the debonding and void growth did indeed occur within the damage zone at the crack tip. The transmission electron micrographs of the RIPS blend containing 6 wt% sPS, shown in Fig. 15, illustrate the differences between the undamaged bulk polymer and the damage zone at the crack tip. Spherical sPS particles, having a diameter of approximately 1–3 μm are clearly seen in the micrograph of the undamaged bulk polymer, see Fig. 3. On the other hand, the micrographs of the thin section taken from the area close to the crack tip, see Fig. 15, show the presence of voids in the damage zone. Such voids could also be observed by optical microscopy. These voids are much larger than the sPS particles, indicating that void growth has indeed occurred after debonding of the sPS. It should be noted that particles are normally not seen in the voids, because they have debonded during testing, and have subsequently fallen out of the voids prior to, or during, the microtoming of the thin sections. However, some particles are still present in the voids in Fig. 15(a), clearly showing the large difference in size between the particles and the voids. The presence of the large voids in the damage zone shows that plastic void growth of the epoxy polymer is a major energy dissipating, and thus toughening micromechanism, in the sPS/epoxy blends with the RIPS microstructure. Elongation of the sPS particles, except for some very limited elongation due to the microtoming process, was not observed in the transmission electron micrographs.

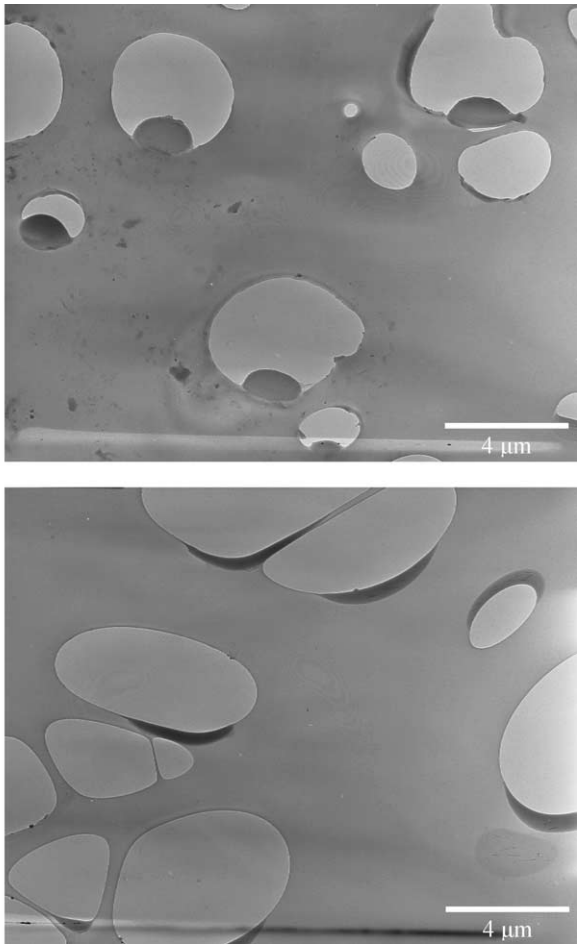

Fig. 15. Transmission electron micrographs of a DN-4PB specimen of the RIPS blend containing 6 wt% sPS. The micrographs show the damage zone at the sub-critical crack tip from two replicate specimens.

In the case where only the spherical sPS particles are responsible for the increase in toughness and fracture energy in the RIPS blends, one would expect an approximately linear increase in these properties as the number and the volume fraction of the particles are increased. The increase in toughness and fracture energy is indeed approximately linear up to around 8 wt% sPS, see Fig. 14. The fracture energy of the RIPS blend containing 8 wt% sPS was somewhat higher than for the 6 wt% sPS blend. However, thin films from the area around the sub-critical crack tip of the 8 wt% blend could not be prepared by microtomy. This is probably due to the high volume fraction of voids in the epoxy matrix, and the thin walls between the voids, which made the samples extremely fragile.

The damage zone at the sub-critical crack tip of the DN-4PB specimens can also be investigated using optical microscopy. As discussed above, the direction of the sub-critical crack in the pure epoxy polymer specimen was straight and there was little evidence of plastic deformation of the epoxy. For the RIPS blends, the sub-critical crack is still relatively straight, confirming the observation of the relatively flat fracture surfaces from using scanning electron microscopy. However, TOM shows a dark area in front of

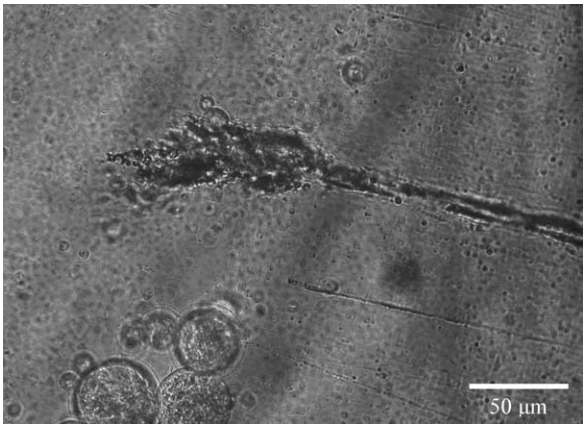

Fig. 16. Transmission optical micrograph of the DN-4PB specimen of the RIPS blend containing 8 wt% sPS, showing the damage zone at the sub-critical crack tip.

the crack tip due to scattering of the transmitted light, see Fig. 16, revealing the region where debonding of the sPS particles, accompanied by plastic void growth, and plastic dilation of the epoxy matrix has occurred. The micrograph shows that the plastic zone is approximately 80 μm at its longest and 30 μm at its widest points. The theoretical size of the plastic zone may be calculated as discussed above. The value of the fracture toughness, K_{Ic}, for the RIPS blend containing 8 wt% sPS was 1.42 $MNm^{-3/2}$. The observed shape of the plastic damage zone ahead of the crack tip is a line-zone, and thus the Dugdale analysis may be employed to model its shape, see Eqs. (5) and (6) earlier. The length of the plastic zone, R, ahead of the crack tip is calculated to be 133 μm, while the crack-opening displacement, δ_t, is 10 μm. Thus, whilst the length and height of the observed plastic zone in Fig. 16 do not agree exactly with the calculations from the Dugdale model, considering the theoretical assumptions and experimental difficulties, the agreement is relatively good.

6.2.3. Toughening micromechanisms of the RIPS blends (above 8 wt% sPS)

At concentrations of sPS higher than 8 wt%, macro phase-separation of sPS occurs, as shown in Fig. 6(a). The size of the macro-phase is typically on a millimetre scale, and it contains a large number of relatively spherical epoxy particles as a result of local phase-inversion. The diameter of these particles is typically 10–50 μm, as shown in Fig. 6(b). However, a relatively low concentration of spherical sPS particles are still present in the epoxy matrix regions of the blend.

The measured fracture energy increases approximately linearly up to 8 wt% sPS, and an apparent maximum is reached at 10 wt%, but upon further addition of sPS the value of G_{Ic} appears to decrease somewhat, as shown in Fig. 14. This decrease coincides with the start of the macro phase-separation of the sPS that takes place above 8 wt%. The reduction in fracture energy arises from two factors. First, the co-continuous structure of the sPS means that the crack must propagate through the sPS phase, which has been shown to exhibit a lower fracture toughness than the pure epoxy [28]. Scanning electron microscopy shows that the surface area of fractured sPS is very small, as the macro-phase sPS is present only as thin shells between the phase-inverted epoxy particles, see Fig. 6(b). Secondly, the macro phase-separated sPS occupies a relatively large volume fraction compared to the spherical sPS particles, due to the local phase-inversion that increases the volume of the co-continuous sPS phase. Thus, there is a large interfacial area between the sPS and the epoxy matrix. Due to the poor adhesion between sPS and epoxy, this interface provides an excellent site for crack propagation. The importance of both factors will increase as the volume fraction of the macro-phase sPS is increased. Hence, a reduction in the measured fracture energy of the RIPS blends would be expected upon an increased concentration of sPS, as is indeed observed.

Interestingly, Pascault and Williams [5] have commented that, where authors have seen an increase in toughness followed by a decrease, this has normally been associated with the formation of a phase-inverted structure where there is poor adhesion between the two phases. For example, McGrail and Street [44] showed that for a thermoplastic additive that could not chemically react with the epoxy resin, the toughness passed through a maximum. However, when the thermoplastic was able to form covalent bonds to the resin, then the measured toughness continued to increase as the thermoplastic concentration was increased.

6.2.4. Toughening micromechanisms of the CIPS blends

For the CIPS blends, the semi-crystalline sPS phase is present as spherulites with an open and pronounced fibrillar substructure in the cured epoxy polymer matrix. The smallest spherulites have a diameter of around 15 μm, while the largest have a diameter of approximately 300 μm.

The fracture energy of the CIPS blend containing 1 wt% sPS is more than double that of the pure epoxy, as shown in Fig. 14. However, the fracture energy only increases relatively slowly above 1 wt% sPS. For example, G_{Ic} = 270 J/m^2 at 1 wt%, and a maximum value of about 350 J/m^2 is measured in the range 8–12 wt% sPS. The measured values of G_{Ic} at high sPS contents are considerably lower than for the RIPS blends, and the fracture energy does not pass through a maximum value as a function of the concentration of sPS. For the CIPS blends, the value of G_{Ic} increases only slowly over the whole range from 1 to 12 wt% of sPS.

The CIPS blends exhibit much coarser and less well-defined fracture surfaces compared with the RIPS blends, see Fig. 7. At lower concentrations of sPS there are both rough and smooth areas on the fracture surfaces, and river markings parallel to the crack growth direction are also visible, see Fig. 7(a). These river markings are caused by crack forking [45]. As the concentration of sPS is increased in the CIPS blends, the surface becomes rougher. Indeed, the smooth areas, and also the river markings, become less common and disappear completely at high concentrations of sPS, see Fig. 7(c) for example. It is difficult to determine how the crack propagates through the CIPS blends using SEM, since it is difficult to distinguish between the sPS and the epoxy phases. In addition, the resolution of the scanning electron microscope is too low for detection of very small features such as the thin crystalline fibrils in the CIPS blends.

Nevertheless, two different types of toughening micro-mechanisms may be identified from the optical micrographs of the DN-4PB specimens of the CIPS blends, as shown in Fig. 17. These are (i) crack deflection, and (ii) microcracking and crack bifurcation; and they are not observed in the corresponding optical micrographs of either the pure epoxy or the RIPS blends.

Crack deflection may be readily observed by comparing the optical micrographs of the CIPS blends, as shown in

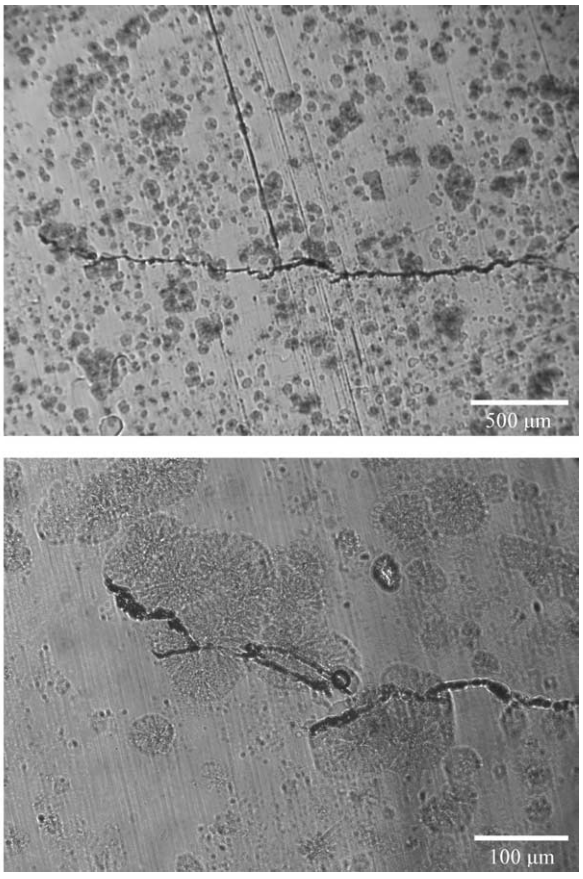

Fig. 17. Transmission optical micrographs of a DN-4PB specimen of the CIPS blend containing 8 wt% sPS. The micrographs show (a) the machined notch and the sub-critical crack; and (b) the tip of the sub-critical crack, where crack deflection and bifurcation are observed. (The direction of the crack growth is from right to left).

Fig. 17, with those of the pure epoxy and the RIPS blends. The pre-made cracks in the pure epoxy and the RIPS samples are virtually straight, normal to the applied tensile stress. Whereas, in the CIPS samples, the crack shows significant deviation from a straight path. When the crack propagates it will tend to take the path with the lowest resistance to crack propagation; and from Fig. 17 it is clear that the spherulitic sPS domains give rise to significant crack deflection. This produces the observed increase in the roughness of the fracture surfaces with increasing concentration of sPS, as shown in Fig. 7, and hence an increase in the true (i.e. local) fracture surface area. Also, when the propagating crack tilts or twists, as it is deflected, it is not loaded in pure mode I, but under a local mixed-mode I/II (tensile/in-plane shear) loading [46]. It is well known that crack propagation under mixed-mode I/II loading requires more energy dissipation than under solely mode I loading. Hence, via either or both of these effects, crack deflection in the CIPS blends will absorb additional energy, and contribute to the observed toughening effect, as is discussed in more detail below.

Microcracking and crack bifurcation were observed close to the sub-critical crack tip, see Fig. 17(b), and also in the wake of the crack tip. Microcracks would appear to form in the spherulitic sPS phase ahead of the main crack tip, and arrest when the crack tip meets the epoxy-matrix phase. These microcracks follow the interface between the sPS fibrils and the epoxy phase within the spherulites, see Fig. 17(b), presumably due to the relatively poor adhesion between the sPS and the epoxy. Hence, the microcracks follow the fibrils, as shown in Fig. 17(b), which do not necessarily run radially from the centre of the spherulite, see Fig. 9 for example. Thus, when the main crack is growing it has several options as to which way it may propagate, and leaves behind some arrested-paths as microcracks in the crack wake; which may or may not be joined to the main crack [47].

Note that the use of optical microscopy shows no evidence of voids sufficiently large to be observed via this technique, see Fig. 17; unlike the case for the RIPS blends. Also, transmission electron microscopy did not give any insight into the toughening micromechanisms of the CIPS blends. In summary, the main mechanisms of toughening for the CIPS blends appear to be (i) crack deflection and (ii) microcracking and bifurcation of the main crack.

6.3. Modelling of the toughening micromechanisms

6.3.1. Modelling of the contribution from the plastic void growth mechanism

It has been shown that debonding and plastic void growth occur for the RIPS blends with a low (i.e. 8 wt% or less) concentration of sPS. The toughening effect of a particulate thermoplastic phase can be predicted using the model by Huang and Kinloch [39]. This model assumes that the fracture specimens behave in a bulk linear-elastic manner, and that the energy dissipation is localised to a small plastic zone at the crack tip, as observed in the present work. Huang and Kinloch postulated that the measured fracture energy of a rubber or thermoplastic modified polymer may be expressed [39] as:

$$G_{Ic} = G_{Icu} + \Psi \tag{5}$$

where G_{Icu} represents the fracture energy of the unmodified epoxy, and Ψ represents the overall toughening contributions. Huang and Kinloch suggested that Ψ was composed of contributions from particle bridging, localised shear banding in the epoxy matrix, and plastic void growth of the epoxy matrix which is initiated by cavitation or debonding of the particulate phase. However, in the present work, microscopy has shown that bridging does not occur, and that the plastic void growth mechanism seems to be by far the dominant toughening micromechanism. Hence the above relationship may be written:

$$G_{Ic} \approx G_{Icu} + \Delta G_v \tag{6}$$

where ΔG_v is the contribution to the increase in fracture energy from plastic void growth of the epoxy matrix. Note

that the adhesion between the sPS and epoxy phases is very poor, and hence debonding can be assumed not to contribute to the toughening effect. The contribution to the increase in fracture energy from the plastic void growth mechanism, ΔG_v, is given [39] by:

$$\Delta G_v = (1 - \mu_m^2/3)(V_{fv} - V_{fr})\sigma_{yc} r_{yu} K_{vm}^2 \quad (7)$$

where μ_m is a material constant, V_{fv} is the volume fraction of voids, V_{fr} is the volume fraction of particles, σ_{yc} is the compressive yield stress of the unmodified epoxy polymer, r_{yu} is the radius of the plastic zone of the unmodified epoxy polymer, and K_{vm} is the maximum stress concentration factor of the von Mises stress in the plastic matrix. The value of the material constant, μ_m, has been reported [48] to be between 0.175 and 0.225, and is normally taken to be 0.2, as reported in [39]. The material properties that were used for calculation of ΔG_v are summarised in Table 2. The maximum stress concentration factor, K_{vm}, was found from a finite element analysis [49] to be 2.22 around a void in an epoxy matrix. (It is assumed that the sPS particles can be treated as voids due to the poor adhesion between the sPS and the epoxy phases). Note that for simplicity this analysis assumes that the plastic zone is circular rather than a Dugdale line-zone. This is a reasonable assumption because the true shape of the plastic zones observed in the present work lies between the circular (Irwin) and Dugdale models.

The RIPS blend containing 6 wt% sPS is considered in detail as an example since all the necessary parameters needed for the equations are known, as given in Table 2. The average diameter of the voids in the damage zone is much larger than the average diameter of the sPS particles in the undeformed bulk polymer. Thus, the volume fraction of voids, V_{fv}, in the epoxy matrix after fracture has occurred is much higher than the volume fraction of particles, V_{fr}, in the epoxy matrix before testing. The measured volume fraction of voids, V_{fv}, was 0.24, while the volume fraction of the particles, V_{fr}, was 0.06. The agreement between the prediction and the experimental fracture energy is very good, see Table 3. The measured toughening increment, Ψ, is 390 J/m^2, while the predicted toughening from the void growth mechanism, ΔG_v, is 410 J/m^2. This confirms that plastic void growth of the epoxy matrix, initiated by a void being formed by the particulate sPS phase debonding, can produce the major increase in the value of the fracture energy, G_{Ic}, recorded in the present work for the RIPS blends.

6.3.2. Modelling of the contribution from crack deflection

For the CIPS blends, the experimental data suggests that crack deflection is occurring, which may contribute significantly to the increase in the fracture energy that arises from the presence of the sPS phase. This mechanism causes an increase in the true (i.e. local) fracture surface area and also causes the crack to grow locally under mixed-mode I/II conditions. It is possible to evaluate the former toughening effect from this mechanism by (i) comparing the measured fracture toughness with the surface roughness, and (ii) to evaluate the latter toughening effect using the analysis by Faber and Evans [46].

Work by Arakawa and Takahashi [50], as reported by Hull [47,51], showed that the toughening effect due to an increase in the true fracture surface area gives a linear relationship between the surface roughness and the overall toughening contribution, Ψ [50]. In the present work, the average surface roughness, R_a, of the compact tension specimens of the CIPS blends, was measured using profilometry. The average roughness of the pure epoxy sample was relatively low, $R_a = 0.02$ μm being measured. The roughness generally increased with an increasing concentration of sPS, from a minimum of 2 μm at 1 wt% sPS to a maximum of 12 μm at a concentration of 12 wt% sPS. These data are shown in Fig. 18, where the measured

Table 2
Material properties of the pure epoxy and the RIPS blend containing 6 wt% sPS

Property	Symbol	Reference	Units	Material	
				Epoxy[a]	6 wt% RIPS
Fracture toughness	K_{Ic}	[b]	MNm$^{-3/2}$	0.73	1.23
Modulus	E	[b]	GPa	2.07	2.20
Poissons ratio	ν	[30]	–	0.35	–
Compressive yield stress	σ_{yc}	[38]	MPa	97.8	–
Plastic zone radius	r_y	[c]	μm	4.7	–
Material constant	μ_m	[39]	–	0.2	–
Volume fraction of rubber	V_{fr}	[b]	–	–	0.24
Volume fraction of voids	V_{fv}	[b]	–	–	0.06

Values are used for calculation of the fracture energy, G_{Ic}, and for the contribution to the increase in fracture energy from the plastic void growth mechanism, ΔG_v.

[a] The pure epoxy was cured at 230 °C as for the RIPS blends.

[b] Measured in the present work.

[c] Calculated using Eq. (2).

Table 3
Measured values of the fracture energy, G_{Ic}, the overall toughening contribution, Ψ, and the calculated contribution to the increase in fracture energy from the plastic void growth mechanism, ΔG_v, for the RIPS blend containing 6 wt% sPS

Property	Symbol	Units	Material	
			Epoxy[a]	6 wt% RIPS
Measured fracture energy	G_{Ic}	J/m^2	230	620
Measured toughening increment	Ψ	J/m^2	–	390
Predicted toughening from void growth	ΔG_v	J/m^2	–	410

[a] The pure epoxy was cured at 230 °C as for the RIPS blends.

roughness is plotted against the overall toughening contribution, Ψ, from the presence of the sPS in the CIPS blends. These do not show a linear relationship, and hence it appears that increases in the true (i.e. local) fracture surface area are not responsible for the increases in the toughness for the CIPS blends.

The measured fracture energies may also be compared to predictions using the analysis by Faber and Evans [46], which considers that crack deflection causes the crack to grow locally under mixed-mode I/II conditions. This analysis uses the shape of the particles, which can be assumed to be spherical in this case, and their volume fraction. The effective volume of the spherulitic sPS domains is much larger than the volume of sPS due to the epoxy that is present between the sPS fibrils. The volume fraction of the spherulitic domains can be calculated from the optical micrographs, see Fig. 8 for example. For the CIPS blend containing 8 wt% sPS, the volume fraction of the spherulitic sPS domains is about 0.30. The Faber and Evans model predicts that the fracture energy for this volume fraction of spheres will be 1.7 times that of the unmodified epoxy. The G_{Ic} of the pure epoxy is 120 J/m^2 and thus the predicted value of G_{Ic} from employing the Faber and Evans model is 200 J/m^2. However, the measured fracture energy of 350 J/m^2 is far higher than this predicted value.

Therefore, whilst crack deflection may contribute significantly to the toughening effect for the CIPS blends, it is not solely responsible for the increased toughness; and microcracking ahead of the crack tip and crack bifurcation may also play a significant role.

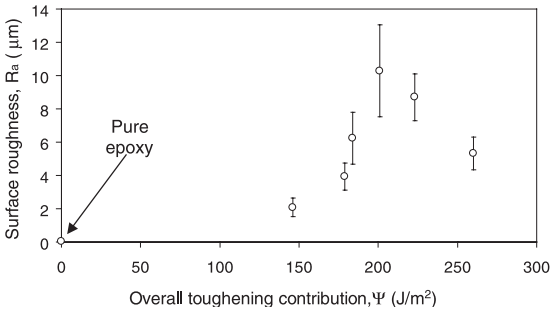

Fig. 18. Average roughness of the fracture surfaces versus measured overall toughening contribution for the pure epoxy polymer, cured at 220 °C, and the CIPS blends.

7. Conclusions

Thermoplastic/epoxy blends were formed using a semi-crystalline thermoplastic, syndiotactic polystyrene (sPS), as the toughening phase. Phase-separation of dissolved sPS from the epoxy occurs via two different routes. First, 'reaction-induced phase-separation' (RIPS) may occur. Here, the curing reaction results in the formation of the three-dimensional epoxy network, forcing the sPS out of solution and leading to the phase-separation of the sPS. Secondly, 'crystallisation-induced phase-separation' (CIPS) may occur. Here, phase-separation of sPS occurs before the epoxy network has been developed sufficiently to force the sPS out of solution. The thermal history of the blend was controlled to produce samples that had undergone phase-separation either by RIPS or by CIPS. For the RIPS blends at low thermoplastic content, the sPS was present as spherical particles, which were 1–4 μm in diameter. For RIPS blends containing more than 8 wt% sPS, macro phase-separation, leading to a co-continuous microstructure with local phase-inversion, occurs. For the CIPS blends, the sPS is pre-crystallised and crystalline spherulites are formed. This microstructure does not change over the range of sPS content studied in the present work.

Dynamic mechanical thermal analysis showed that the initially soluble sPS has totally phase-separated from the cured epoxy, and that no sPS was present in the epoxy polymer phase(s). For the CIPS blends, the sPS is in a highly crystalline state, and hence a high T_g for the sPS phase is measured. For the macro phase-separated RIPS blends, the sPS is of a lower crystallinity, resulting in a T_g equal to that of the bulk material. The spherical RIPS particles of sPS have the lowest T_g, and these appear to be relatively amorphous.

The fracture toughness, K_{Ic}, of the blends was measured. The pure epoxy polymer is very brittle with K_{Ic} values of about 0.65 MNm$^{-3/2}$, which is typical of a brittle thermosetting epoxy polymer. The addition of merely 1 wt% sPS gives an immediate increase in toughness. A value of about 0.81 MNm$^{-3/2}$ is recorded for both the RIPS and the CIPS blends. However, above 3 wt% sPS the measured fracture toughness for the RIPS and CIPS blends differs markedly. For the RIPS blends there is a steady increase in toughness with increasing content of sPS, and a maximum value of $K_{Ic}=1.42$ MNm$^{-3/2}$ is obtained at 8 wt% sPS; with the relationship between K_{Ic} and wt% sPS being linear. Above 8 wt% sPS, the measured toughness starts to decrease somewhat. On the other hand, the measured toughness of the CIPS blends increases only slightly for higher concentrations of sPS above 1 wt% sPS.

Hence, the toughness of the CIPS blends does not reach a maximum value in the same way as the K_{Ic} values do for the RIPS blends. The measured toughness values for the CIPS blends are approximately constant, within experimental error, over the range from about 1–12 wt% sPS used in the present work. For example, a value of $K_{Ic}=0.83\ MNm^{-3/2}$ was measured for the CIPS blend containing 1 wt% sPS, and a K_{Ic} of $0.93\ MNm^{-3/2}$ was measured for the CIPS blend containing 8 wt% sPS. In addition, the measured toughness values are much lower than those for the RIPS blends. The fracture energy, G_{Ic}, of the blends was calculated from the measured fracture energy and modulus, and the data show similar trends to the K_{Ic} values.

Microscopy was used to identify the toughening micromechanisms. For the RIPS blends, debonding of the sPS and epoxy phases and plastic void growth of the epoxy matrix occur. Debonding absorbs little or no energy because the adhesion between the sPS and epoxy phases is very poor. Thus, the dominant energy-absorbing micromechanism is the subsequent plastic void growth in the epoxy matrix, and this was predicted using an analytical model. The agreement between the experimental data and the theoretical predictions was found to be very good. In the case of the CIPS blends, the main toughening mechanisms identified were (i) crack deflection, and (ii) microcracking and crack bifurcation. Of particular importance is the deflection of the main propagating crack, which results in an increased roughness of the fracture surfaces and hence local mixed-mode I/II crack growth occurring, which requires more energy dissipation than solely mode I loading. However, quantitative calculations also revealed that microcracking ahead of the crack tip and crack bifurcation may also play a significant role in increasing the toughness of the CIPS blends.

Acknowledgements

The authors gratefully acknowledge the financial support provided through the European Community's Human Potential Programme under contract HPRN-CT-2000-00146, PolyNetSet. They would also like to thank Pierre Alcouffe at INSA de Lyon for performing the microtoming, and Dr Jaap Schut at IPF Dresden/INSA de Lyon for fruitful discussions. Dr Ambrose Taylor is a Royal Academy of Engineering Research Fellow, and he would like to thank the Royal Academy of Engineering for their support.

References

[1] Kinloch AJ. MRS Bulletin 2003;(28):445–8.
[2] Rowe EH, Siebert AR, Drake RS. Mod Plastics 1970;47:110–7.
[3] Kinloch AJ, Shaw SJ, Hunston DL. Polymer 1983;24:1355–63.
[4] Pearson RA, Yee AF. J Mater Sci 1986;21:2475–88.
[5] Pauscault JP, Williams RJJ. Formulation and characterization of thermoset-thermoplastic blends. In: Paul DR, Bucknall CB, editors. Polymer blends volume 1: formulation. New York: Wiley; 1999. p. 379–415.
[6] Bucknall CB, Partridge IK. Polymer 1983;24:639–44.
[7] Bucknall CB, Gilbert AH. Polymer 1989;30:213–7.
[8] Kim SC, Brown HR. J Mater Sci 1987;22:2589–94.
[9] MacKinnon AJ, Jenkins SD, McGrail PT, Pethrick RA. Macromolecules 1992;25:3492–9.
[10] Kinloch AJ, Yuen ML, Jenkins SD. J Mater Sci 1994;29:3781–90.
[11] Kinloch AJ, Taylor AC. J Mater Sci 2003;38:65–79.
[12] Hedrick JC, Patel NM, McGrath JE. Toughening of epoxy resin networks with functionalized engineering thermoplastics. In: Riew CK, Kinloch AJ, editors. Toughened plastics I: science and engineering. Washington: American Chemical Society; 1993. p. 293–304.
[13] Hodgkin JH, Simon GP, Varley RJ. Polym Adv Technol 1998;9:3–10.
[14] Pearson RA. Toughening epoxies using rigid thermoplastic particles. In: Riew CK, Kinloch AJ, editors. Toughened plastics I: science and engineering. Washington: American Chemical Society; 1993. p. 405–25.
[15] Hourston DJ, Lane JM. Polymer 1992;33:1379–83.
[16] Girard-Reydet E, Vicard V, Pauscault JP, Sautereau H. J Appl Polym Sci 1997;65:2433–45.
[17] Biolley H, Pascal T, Sillion B. Polymer 1994;35:558–64.
[18] Hedrick JL, Yilgor I, Wilkes GL, McGrath JE. Polym Bull 1985;13:201–8.
[19] Yoon TH, Priddy DB, Lyle GD, McGrath JE. Macromol Symp 1995;98:673–86.
[20] Girodet C, Espuche E, Sautereau H, Chabert B, Ganga R, Valot E. J Mater Sci 1996;31:2997–3002.
[21] Cardwell BJ, Yee AF. J Mater Sci 1998;33:5473–84.
[22] Kinloch AJ, Taylor AC. J Mater Sci 2002;37:433–60.
[23] Ishihara N, Seimiya T, Kuramoto M, Uoi M. Macromolecules 1986;19:2464–5.
[24] Malanga M. Adv Mater 2000;12:1869–72.
[25] Schut J, Stamm M, Dumon M, Gerard J-F. Macromol Symp 2003;198:355–62.
[26] Schut J, Stamm M, Dumon M, Galy J, Gerard J-F. Macromol Symp 2003;202:25–35.
[27] Schut J. Blends of syndiotactic polystyrene and thermoset epoxy resin: engineering and characterization. PhD thesis, INSA de Lyon, France; 2003.
[28] Korenberg CF, Kinloch AJ, Taylor AC, Schut J. J Mater Sci Lett 2003;22:507–12.
[29] ISO13586:2000(E): Plastics—determination of fracture toughness (G_{IC} and K_{IC})—Linear elastic fracture mechanics (LEFM) approach.
[30] Kinloch AJ. Adhesion and adhesives: science and technology. Chapman & Hall: London; 1987. Chapter 7.
[31] Holik AS, Kambour RP, Hobbs SY, Fink DG. Microstruct Sci 1979;7:357–67.
[32] Sue H-J. Polym Eng Sci 1991;31:271–4.
[33] Sue H-J. Polym Eng Sci 1991;31:275–88.
[34] Sue H-J, Yee AF. J Mater Sci 1992;28:2975–80.
[35] Lee J, Yee AF. Polymer 2000;41:8363–73.
[36] Kawaguchi T, Pearson RA. Polymer 2003;44:4229–38.
[37] Kinloch AJ, Young RJ. Fracture behaviour of polymers. Chapman & Hall: London; 1983. Chapter 3.
[38] Salmon N. Personal communications; 2002–4.
[39] Huang Y, Kinloch AJ. J Mater Sci 1992;27:2763–9.
[40] Erickson BL, Asthana H, Drzal LT. J Adhesion Sci Technol 1997;11:1249–67.
[41] Billmeyer Jr FW. Textbook of polymer science. 3rd ed. Singapore: Wiley; 1984. Chapter 12.
[42] Dutt G, Kit KM. J Appl Polym Sci 2003;87:1975–83.
[43] Tercjak A, Remiro PM, Mondragon I. Polym Eng Sci 2005;45:303–13.
[44] McGrail PT, Street AC. Macromol Symp 1992;64:75–84.

[45] Andrews EH. Fracture in polymers. Edinburgh: Oliver and Boyd; 1968. Chapter 6.
[46] Faber KT, Evans AG. Acta Metall 1983;31:565–76.
[47] Hull D. Fractography: observing, measuring and interpreting fracture surface topography. Cambridge: Cambridge University Press; 1999. Chapter 5.
[48] Sultan JN, McGarry FJ. Polym Eng Sci 1973;13:29–34.
[49] Huang Y, Kinloch AJ. J Mater Sci 1992;27:2753–62.
[50] Arakawa K, Takahashi K. Int J Frac 1995;48:103–14.
[51] Hull D. J Mater Sci 1996;31:4483–92.